Spectrochimica Acta Part A: Molecular and Biomolecular Spectroscopy 244 (2021) 118829

Contents lists available at ScienceDirect

Spectrochimica Acta Part A: Molecular and Biomolecular Spectroscopy

journal homepage: www.elsevier.com/locate/saa

Computational investigation of molecular structures, spectroscopic properties and antitumor-antibacterial activities of some Schiff bases

Serpil Kaya, Sultan Erkan, Duran Karakaş *

Sivas Cumhuriyet University, Science Faculty, Chemistry Department, 58140 Sivas, Turkey

ARTICLE INFO

Article history:
Received 27 May 2020
Received in revised form 29 July 2020
Accepted 9 August 2020
Available online 18 August 2020

Keywords:
Schiff bases
Spectroscopic features
Antitumor-antibacterial activity
Computational research

ABSTRACT

Molecular structures, spectroscopic properties (IR, ^{1}H NMR and ^{13}C NMR, UV-VIS), molecular electrostatic potential maps and some molecular properties (ionization energy, electron affinity, energy gap, hardness, electronegativity, electrophilicity index, static dipole moment and average linear polarizability) of three Schiff bases which are 2-((ethylamino)methyl)-6-methoxyphenol (**HL1**), 2-((ethylamino) methyl)-6-methylphenol (**HL2**) and 2-((ethylamino)methyl)-6-chlorophenol (**HL3**) were computed at B3LYP/6-31G(d) level in aqueous phase. The effects of methoxy, methyl and chloro substituents on Schiff bases were examined and it was found that the electron donating property of methyl and chlorine substituents was higher than the methoxy substituent. In order to investigate the antitumor activities of Schiff bases were docked against the breast cancer (MCF7) cell line. Molecular docking results were compared with antitumor standard 5-fluorouracil. Antitumor activity of HL2 and HL3 molecule was found to be higher than HL1 against MCF-7 cell line. In addition, in order to predict the antibacterial activities of Schiff bases were docked against the *Mycobacterium tuberculosis* (H37Rv) cell line. Docking results were compared with the antibacterial reference N-(salicylidene)-2-hydroxyaniline. Antibacterial activity of HL2 and HL3 molecules was found to be higher than HL1. It is estimated that the binding of the electron donating group to the ortho position of the hydroxyl group in studied Schiff bases increases both antitumor and antibacterial activity.

1. Introduction

Compounds containing the azomethine group ($R_2C{=}NR'$, $R' \neq H$) are known as Schiff bases. Schiff bases are synthesized by reaction of primary amines with an aldehyde or ketone under special conditions. They have high stability and form highly stable complexes with transition metal ions [1].

Schiff bases and their metal complexes have gained considerable importance in medicine because of their biological, pharmacological, antitumor properties and their ability to form chelates [2–5]. Schiff bases are the most commonly used compounds as pigment, dye, catalyst and polymer stabilizer [6]. In addition, Schiff bases have been reported to exhibit a wide range of biological activities such as antifungal, antibacterial, antimalarial, including antiproliferative, anti-inflammatory, antiviral and antipyretic [6,7]. Imine or azomethine groups are present in various natural compounds, naturally derived compounds and unnatural compounds. Imine or azomethine groups in such compounds are critical for their biological activity [8–10].

Schiff bases are ligands commonly used in coordination chemistry. Imine nitrogen is basic and exhibits π-receptive properties [11]. It is known that these ligands form the σ-bond by giving the metal ion a lone pair on the nitrogen and form the π-bond by taking electrons from the metal to the C═N π* molecular orbital. In the case of a second functional group that is close to the azomethine group and can be deprotonized, Schiff bases act as a bidentate ligand forming complex compounds. Generally, the functional group that is close to the azomethine group is an OH group.

Transition metal complexes attract great attention due to applications in areas such as antibacterial, anticancer and flame retardant [12–16]. The success of coordination complexes in cancer treatment has been continuing since the discovery of cisplatin. Cisplatin remains the most widely used and best-selling anticancer drug in the world in chemotherapy [17–20]. However, cisplatin and cisplatin-like drugs such as carboplatin and oxaliplatin have serious side effects such as toxicity and drug resistance development [21]. In recent years, pharmacists and bioinorganic chemists have designed new metal-based anticancer drugs due to the aforementioned disadvantages of chemotherapeutic drugs. These anticancer drugs had low toxicity, good selectivity and good biological activity [22].

Schiff base metal complexes are of great interest due to their wide range of application areas such as antituberculosis, antineoplastic, antimalarial, anticancer, antioxidant, antifungal, anti-inflammatory, corrosion inhibition and anti-inflammatory activity [23–27].

* Corresponding author.
E-mail address: dkarakas@cumhuriyet.edu.tr (D. Karakaş).

https://doi.org/10.1016/j.saa.2020.118829
1386-1425/

Although the syntheses and characterizations of Schiff bases and their transition metal complexes have been successfully done and many properties have been determined experimentally, it is clear that this is costly and time consuming. Therefore, there is a great interest in computational studies on complex compounds. Because, without making syntheses of complexes, their structure can be calculated and IR, NMR and UV-VIS spectra can be obtained directly for their characterizations. In addition, electronic structures and many molecular properties can be estimated by calculation [28,29].

In this study, we aimed to investigate the structural, electronic, molecular, antitumor and antibacterial properties of HL1, HL2 and HL3 Schiff bases computationally. Of these compounds, only HL1 Schiff base has been experimentally synthesized and its antitumor property has been studied by Si-Jie Li et al. [30]. HL2 and HL3 Schiff bases are hypothetical. Antitumor properties of Schiff bases were compared with 5-fluorouracil (5-FU) and antibacterial properties with N-(salicylidene)-2-hydroxyaniline (SHA). The binding of CH_3O, CH_3 and Cl substituents to the ortho position of the hydroxyl group, the change of molecular properties, antitumor and antibacterial activities were investigated.

2. Computational procedure

The molecular structures of HL1, HL2 and HL3 Schiff bases were drawn in the GaussView 6.0.16 program [31]. Optimization and vibration frequency calculations were made at B3LYP/6-31G(d) level in Gaussian 09: AS64L-G09RevD.01 program and no imaginary frequency was obtained [32,33]. B3LYP is a hybrid density functional theory method [34] and 6-31G(d) is a polarized basis set [35]. In general, as biological events occur in the aqueous phase, calculations were made in the aqueous phase using the conductor-like polarizable continuum (C-PCM) model [36]. NMR spectrums were calculated at the same level by Gauge-including atomic orbitals (GIAO) method [37], and UV-VIS spectrums at the same level by time-dependent density functional theory (TD-DFT) method [38]. Average molecular polarizability (α), static dipole moment (μ), HOMO energy (E_{HOMO}) and LUMO energy (E_{LUMO}) were taken from the output file. Some electronic structure descriptors such as ionization energy (I), electron affinity (A), energy gap (AE), hardness (η), absolute electronegativity (χ) and electrophilicity index (ω) were calculated using Eqs. (1)–(6) [39,40].

$$I = -E_{HOMO} \tag{1}$$

$$A = -E_{LUMO} \tag{2}$$

$$\Delta E = E_{LUMO} - E_{HOMO} \tag{3}$$

$$\eta = \frac{I-A}{2} \tag{4}$$

$$\chi = \frac{I+A}{2} \tag{5}$$

$$\omega = \frac{\mu_{cp}^2}{2\eta} \tag{6}$$

Schiff bases and antitumor standard 5-FU were docked against the breast cancer cell line MCF-7 (PDB ID: 1JNX). In addition, Schiff bases and antibacterial reference SHA [41] were docked against the tuberculosis bacteria cell line H37Rv (PDB ID: 3TZ6). Molecular docking calculations were performed at Docking Server program [42].

Table 1
^{1}H NMR chemical shift values (ppm) and correlation coefficients (R^2) calculated at levels 1–9 for HL1 Schiff base.

Level	C13*H*	C12*H*	C22*H*	C3*H*	C4*H*	C2*H*	C10*H*	R^2
1)	1.24	3.17	3.56	7.00	7.25	7.32	9.02	0.9931
2)	1.16	3.79	4.12	6.83	6.93	7.06	8.29	0.9961
3)	1.20	3.83	4.11	7.01	7.03	7.14	8.39	0.9964
4)	1.24	3.18	3.64	6.35	6.58	6.59	8.40	0.9921
5)	1.07	3.06	3.49	6.32	6.48	6.52	8.00	0.9972
6)	2.05	4.10	4.64	7.61	7.79	7.82	9.47	0.9959
7)	1.27	3.30	3.62	7.09	7.20	7.25	9.10	0.9923
8)	1.04	3.18	3.51	7.09	7.12	7.18	8.62	0.9952
9)	1.16	3.10	3.57	7.24	7.26	7.45	8.89	0.9913
Exp.	1.18	3.59	3.83	6.87	7.04	7.33	8.54	

3. Findings and discussion

3.1. Benchmark analysis

The process of determining the most suitable level for a quantum chemical calculation is called benchmark analysis. In order to perform benchmark analysis, various levels are created by considering the molecule whose properties will be calculated. At considered levels, an experimentally measured property of the molecule is calculated. The compatibility between the calculated feature and the experimentally measured feature is investigated. The level that gives the best fit is determined as the calculation level.

For HL1 only, ^{1}H NMR chemical shift values and IR spectrum were experimentally measured by Si-Jie Li et al. [30]. Peak labeling and peaks frequencies are not given in experimental IR spectrums. Therefore, ^{1}H NMR chemical shift values were used for benchmark analysis. ^{1}H NMR chemical shift values of HL1 Schiff base were calculated at the following nine levels: 1) HF/6-31G 2) HF/6-31G(d), 3) HF/6-31G+(d, p) 4) B3LYP/6-31G, 5) B3LYP/6-31G(d), 6) B3LYP/6-31G+(d,p), 7) M062X/6-31G, 8) M062X/6-31G(d) ve 9) M062X/6-31+G(d,p) Gauge-including atomic orbitals (GIAO) method was chosen in ^{1}H NMR calculations. Chemical shift values were obtained according to the tetramethylsilane (TMS) standard. Experimental values were plotted against the calculated values and correlation coefficients (R^2) were calculated. ^{1}H NMR chemical shift values, experimental values and correlation coefficients (R^2) calculated at the given levels are presented in Table 1.

The closer the correlation coefficient (R^2) is to 1.0, the better the correlation between experimental and computational data is said to be. When the correlation coefficients (R^2) given in Table 2 are examined,

Table 2
Some bond lengths (Å) and bond angles (^{0}) of Schiff bases calculated at B3LYP/6-31G (d) level in aqueous phase.

	HL1	HL2	HL3
Bond length			
C1-C6	1.418	1.411	1.406
C6-O17	1.348	1.350	1.340
O17-H18	1.006	1.006	1.011
C5-C10	1.460	1.459	1.461
C10-N11	1.285	1.285	1.283
N11-C12	1.457	1.457	1.457
C1-O26(C22, Cl22)	1.365	1.508	1.760
N11···H18	1.704	1.704	1.681
Bond angle			
C6-O17-H18	106.14	106.69	106.40
C6-C1-C2	119.68	118.20	121.56
C1-C6-O17	118.24	118.03	119.96
C5-C6-O17	122.34	121.39	122.00
C5-C10-N11	122.51	122.46	122.07
C6-C5-C10	120.51	121.03	120.29
C10-N11-C12	119.43	119.49	119.68

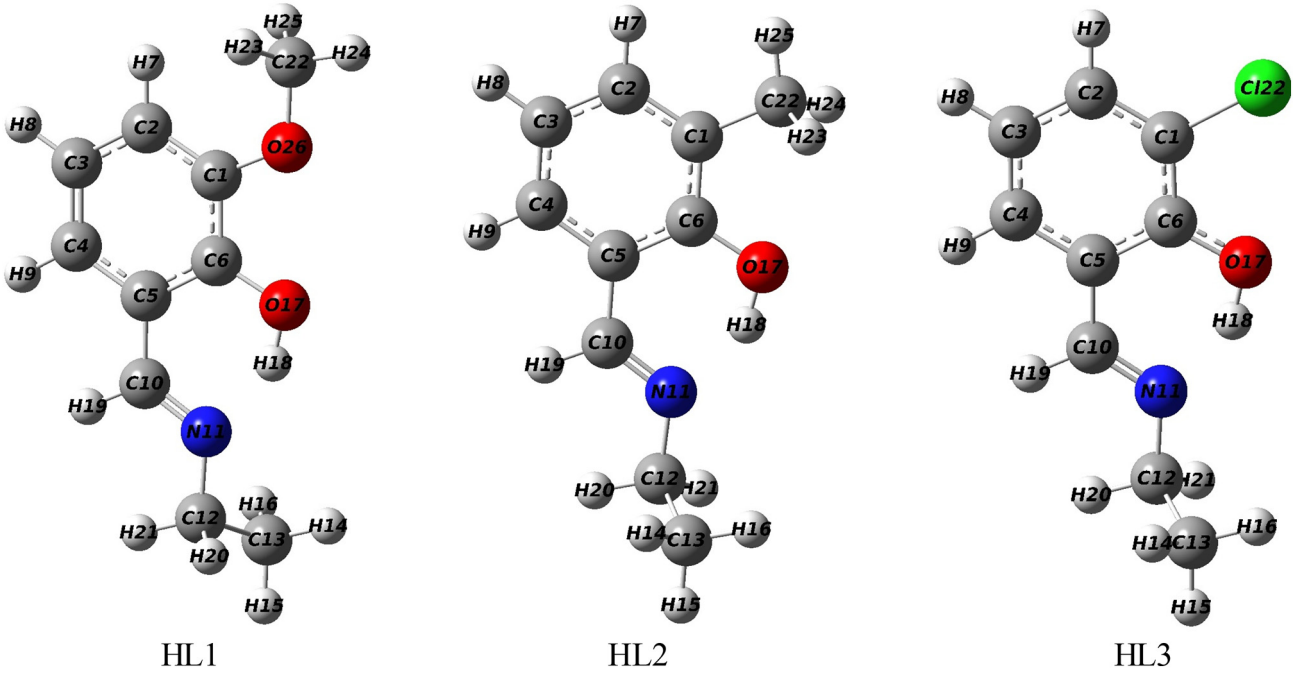

Fig. 1. Optimized structures of HL1, HL2 and HL3 Schiff bases at B3LYP/6-31G (d) level in aqueous phase.

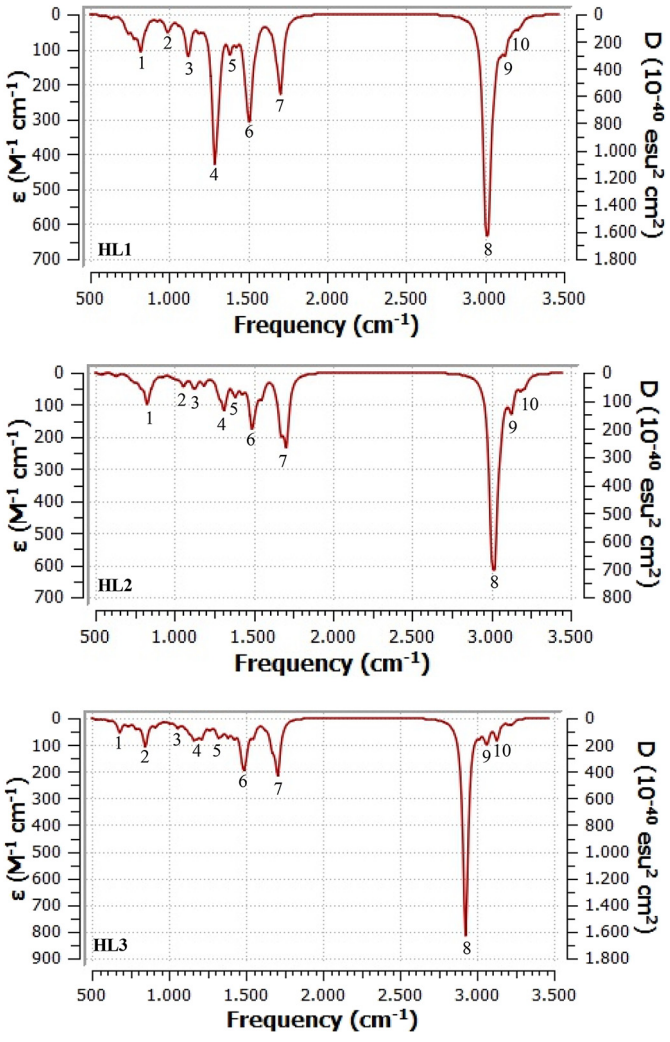

Fig. 2. IR spectra of HL1, HL2 and HL3 Schiff bases calculated at B3LYP/6-31G(d) level in aqueous phase.

it is seen that the correlation coefficients of all levels are very close to 1.0. This result shows that almost all of the levels considered can be used in the computational examination of the HL1 ligand. However, it is seen that the closest to 1.0 is obtained at B3LYP/6-31G(d) level. Thus, considering the ^{1}H NMR chemical shift values of the HL1 Schiff

Table 3
Some vibration frequencies and labeling of Schiff bases calculated at B3LYP/6-31G(d) level in aqueous phase.

Schiff base	Peaks	Mode	Frequency (cm^{-1})	Labeling
HL1	1	24	819.1	T (H-O-C-C)
	2	30	988.9	S (C—H), S (C—C), S (O—C)
	3	34	1121.8	S (O—C)
	4	41	1287.9	S (C—C), S (O—C), B (H-C-C)
	5	45	1385.0	B (C—H)
	6	50	1506.0	B (H-C-H)
	7	59	1705.8	S (N—C)
	8	61	3023.3	S (O—H), S (C—H)
	9	68	3128.2	S (C—H)
	10	71	3210.6	S (C—H)
HL2	1	23	827.8	T (H-O-C-C)
	2	30	1054.3	S (N—C), S (C—C)
	3	34	1132.8	S (N—C), T (H-C-C-N)
	4	39	1306.3	B (H-C-N), T (H-C-N-C)
	5	42	1383.0	B (H-C-N), B (H-C-H), T (H-C-N-C)
	6	47	1488.8	S (C—C), B (H-O-C), B (H-C-C)
	7	56	1706.2	S (N—C)
	8	58	3023.4	S (O—H), S (C—H)
	9	64	3126.4	S (C—H)
	10	69	3212.6	S (C—H)
HL3	1	18	679.9	S (Cl—C), B (N-C-C), B (C-C-C)
	2	23	847.3	T (H-O-C-C)
	3	29	1057.5	S (N—C), S (C—C)
	4	33	1186.3	B (H-C-N), T (H-C-C-N)
	5	37	1320.9	S (C—C), S (O—C), B (H-C-C)
	6	43	1490.1	S (O—C), B (H-C-C)
	7	50	1707.2	S (N—C)
	8	51	2926.0	S (O—H), S (C—H)
	9	53	3056.0	S (C—H)
	10	56	3128.5	S (C—H)

B: Bending, T: Torsion, S: Stretching.

base, it can be said that the level of B3LYP/6-31G(d) will yield optimal results for such compounds.

3.2. Molecular structures

The ground state optimization structures of the studied Schiff bases were obtained in the aqueous phase at B3LYP/6-31G(d) level and are given in Fig. 1.

Some molecular structure parameters (bond lengths and bond angles) of the Schiff bases examined are given in Table 2. As can be seen from the bond lengths in Table 2, there are no significant differences in the bond lengths considered by binding one of the CH_3O, CH_3 and Cl groups to the ortho position of the hydroxyl group. However, while the length of the O—H bond increases slightly in the HL3 molecule, the N…H hydrogen bond length decreases slightly. This is a result of the inductive effect of chlorine. In all molecules, C1-C6 lengths are about 1.41 Å while C5-C10 lengths are about 1.46 Å. A similar situation exists between N11-C12 and C10-N11. It can be said that these length differences are caused by the bond degrees. The C6-O17-H18 bond angles being around 106° indicate that the oxygen atom has four siteric numbers. C6-O17-H18 bond angles are smaller than ideal tetrahedral angle (109.5°) due to the high repulsion of two lone pairs. Angles C6-C1-C2, C1-C6-O17, C5-C6-O17, C5-C10-N11, C6-C5-C10 and C10-N11-C12 are very close to ideal triangular plane angles (120°). The angle C10-N11-C12 is slightly less than 120° because the lone pair-bond pair repulsion is larger than the bond pair-bond pair repulsion.

3.3. IR spectrums and labeling of peaks

The vibration spectrums of Schiff bases were calculated to verify molecular structures. Ten high intensity peaks were considered for each molecule. High intensity peaks are given in Fig. 2. As seen in Fig. 2, IR spectrums of Schiff bases are generally similar. Unlike HL1 and HL2, there is a peak at low frequency (679.9 cm^{-1}) due to the C—Cl stretching vibration for HL3. The harmonic vibration frequencies and labeling of the peaks given in Fig. 2 are shown in Table 3.

The most prominent feature of Schiff bases is that it contains C═N bond. The peak of the stretching vibration of this bond is the number 7 peak for three molecules. C═N harmonic bond stretching frequencies for HL1, HL2 and HL3 were found to be 1705.8, 1706.2 and 1707.2 cm^{-1}, respectively. Fundamental scale factor for B3LYP/6-31G(d) level is given as 0.952 [43]. When the calculated values are multiplied by this scale factor, 1623.9, 1624.3 and 1625.2 cm^{-1} values are obtained, respectively. Depending on the environment in which the Schiff bases were found, the C═N stretching frequencies were obtained experimentally in the range of 1612–1632 cm^{-1} [44]. According to these findings, the

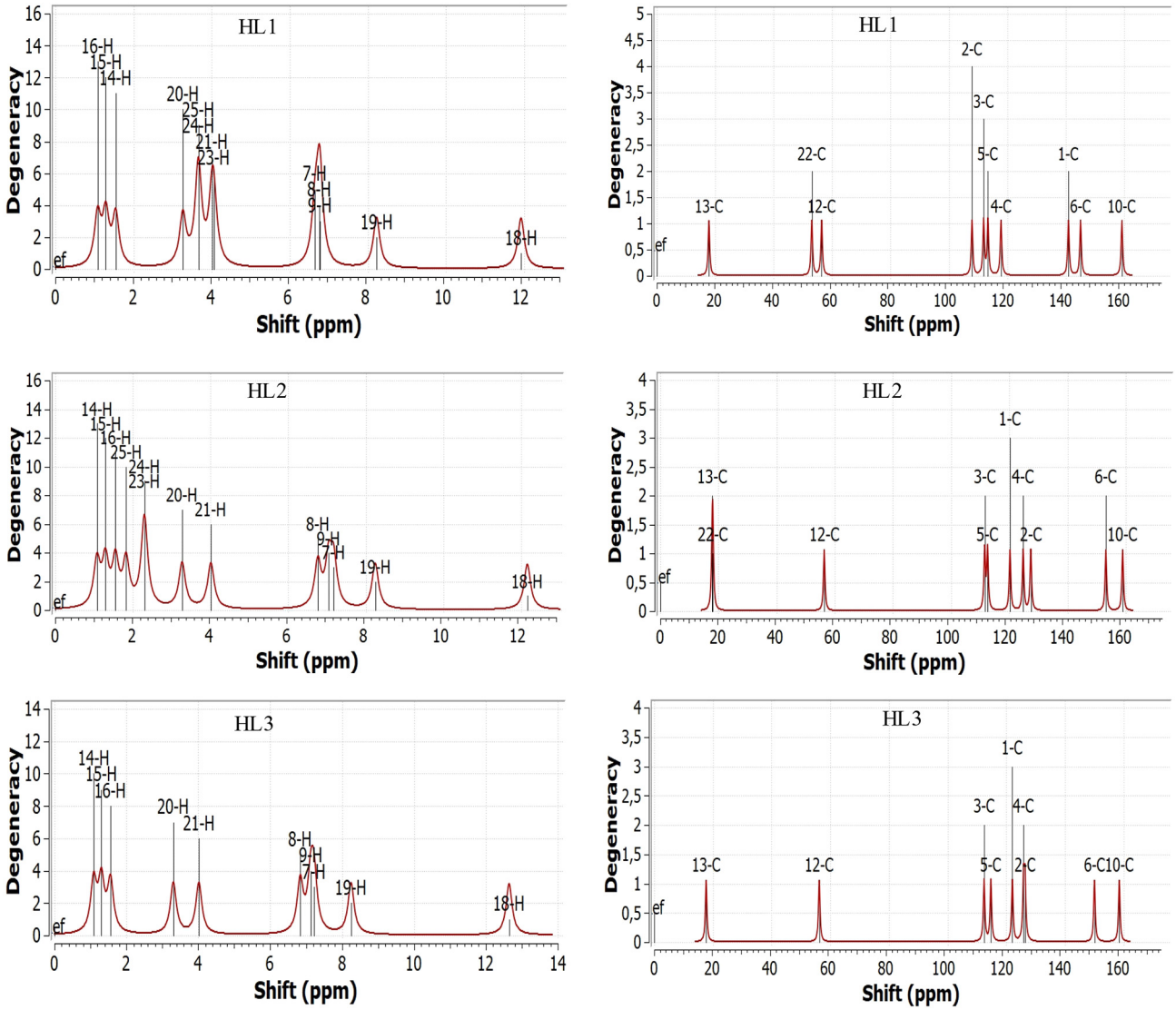

Fig. 3. ^{1}H NMR and ^{13}C NMR spectrums of Schiff bases calculated at GIAO-B3LYP/6-31G(d) level in aqueous phase. See Fig. 1 for atomic labeling.

calculated C═N stretching frequencies seem to be quite compatible with experimental values.

O—H stretching frequencies are generally observed at frequencies higher than 3200 cm^{-1}. In this study, O—H stretching frequencies were calculated as approximately 3023 cm^{-1} for HL1 and HL2 and 2926 cm^{-1} for HL3. This is due to the formation of intramolecular hydrogen bond in the form of O-H… N. Hydrogen bond formation weakens the O—H bond strength and causes the stretching frequency to drop. This result is also compatible with the bond lengths given in Table 2. As seen in Table 2, N11… H18 hydrogen bond length was shortened and O—H bond length increased for HL3. This explains both the behavior of HLn-type Schiff bases as bidentate ligands and their binding from N and O atoms.

Peaks 9 and 10 belong to C—H stretching vibrations. It was generally calculated around 3100–3200 cm^{-1}. Other C—C, C—N, O—C single bond stretching vibrations and some torsions and bending vibrations occurred in the single bond stretching region (800–1500 cm^{-1}) as expected. According to the basic relation of the vibration spectra, the higher reduced mass of the C—Cl bond caused it to emerge at the lower frequency.

3.4. NMR spectrums and labeling of peaks

For structural characterization, ^{1}H NMR and ^{13}C NMR spectra of Schiff bases were calculated and peaks were labeled. Chemical shifts were given according to the TMS reference. Shieldings were calculated as 32.18 ppm for TMS proton and 189.71 ppm for TMS carbon. Chemical shift values of Schiff bases ^{1}H NMR and ^{13}C NMR were calculated from $\delta = \Sigma_{TMS}-\Sigma$ relation. Here Σ_{TMS} is the shielding of proton or carbon in TMS, Σ is the shielding of proton or carbon in the sample. The ^{1}H NMR and ^{13}C NMR spectra of Schiff bases were calculated at GIAO-B3LYP/6-31G(d) level in the aqueous phase and are given in Fig. 3.

As can be seen from Fig. 3, it is seen that ^{1}H NMR spectrums are quite similar for HL1, HL2 and HL3 molecules. The same can be said for the ^{13}C NMR spectra. This finding indicates that the molecular structure of the Schiff bases investigated is very similar. Chemical shifts of ^{1}H and ^{13}C NMR are given in Table 4.

As can be seen from Fig. 3 and Table 4, there are four groups of hydrogen in the studied molecules. These are phenol group hydrogen (H18), azomethine group hydrogen (H19), aromatic ring hydrogen (Ar—H) and hydrogens bound to aliphatic carbon atoms (Al—H). Their chemical shift values (δ) increase in the following order: δ(Al—H) < δ(Ar—H) < δ(H19) < δ(H18) (Fig. 3, Table 4). This order is compatible with the shielding principle of nuclear magnetic resonance spectroscopy. According to the shielding principle, the less shielded nucleus has a high chemical shift value. Factors such as inductive effect, electronegativity, and hybridization affect shielding of nucleus [45]. H18 is attached to the oxygen atom with high electronegativity and its core is less shielded. H19 is less shielded as it is both attached to the carbon atom with high s-character and adjacent to the nitrogen atom with high electronegativity. On the other hand, the hydrogens in Al—H are highly shielded. Because they are attached to carbon atoms with low s-character hybridization (sp^3). Therefore, they have a low ppm value.

Among the ^{13}C NMR spectrum and chemical shift values, *C10* has the highest chemical shift value. As seen in Fig. 1, *C10* carbon is azomethine group carbon. Azomethine carbon neighbors both nitrogen atom with high electronegativity and has made hybridization with sp^2. Both factors cause *C10* carbon to be shielded less. Less shielded nucleus has high chemical shear value. This result is compatible with the literature [46,47]. Aromatic ring carbons (*C1*, *C2*, *C3*, *C4*, *C5*, *C6*) that make sp^2 hybridization have lower chemical shift values than azomethine carbon and their chemical shifts vary according to their proximity to the electronegative atom. Since *C6* carbon is adjacent to the electronegative OH group, its chemical shift is higher than *C1*, *C2*, *C3*, *C4* and *C5*. *C12*, *C13*, and *C22* are aliphatic carbons, these have sp^3 hybridization and their nuclei are highly shielded. Highly shielded cores have low chemical shift values.

Chemical shifts of *C1* in HL1, HL2 and HL3 Schiff bases were obtained as 140.9, 120.2 and 122.0 ppm, respectively. According to the calculated chemical shift values, the electron withdrawing order of CH_3O, CH_3 and Cl groups should be CH_3 < Cl < CH_3O in the aqueous phase. In the case of CH_3 and Cl binding, the *C1* chemical shift values are close, indicating that

Table 4
^{1}H NMR and ^{13}C NMR chemical shift values of Schiff bases calculated at GIAO-B3LYP/6-31G(d) level in aqueous phase.

^{1}H NMR chemical shift (ppm)				^{13}C NMR chemical shift (ppm)			
Labeling	HL1	HL2	HL3	Labeling	HL1	HL2	HL3
H7	6.65	7.17	7.22	*C1*	140.91	120.21	122.02
H8	6.76	6.76	6.83	*C2*	107.90	124.72	126.35
H9	6.76	7.04	7.13	*C3*	111.90	111.51	112.40
H14	1.08	1.07	1.10	*C4*	117.83	124.72	125.85
H15	1.29	1.29	1.30	*C5*	113.35	112.49	114.70
H16	1.54	1.55	1.56	*C6*	145.05	153.15	150.01
H18	11.92	12.16	12.64	*C10*	159.20	158.92	158.46
H19	8.22	8.24	8.25	*C12*	56.43	56.35	56.23
H20	3.26	3.27	3.31	*C13*	17.85	17.88	17.68
H21	4.05	4.01	4.02	*C22*	53.06	18.06	–
H23	3.66	2.30	–				
H24	4.00	2.30	–				
H25	3.66	1.82	–				

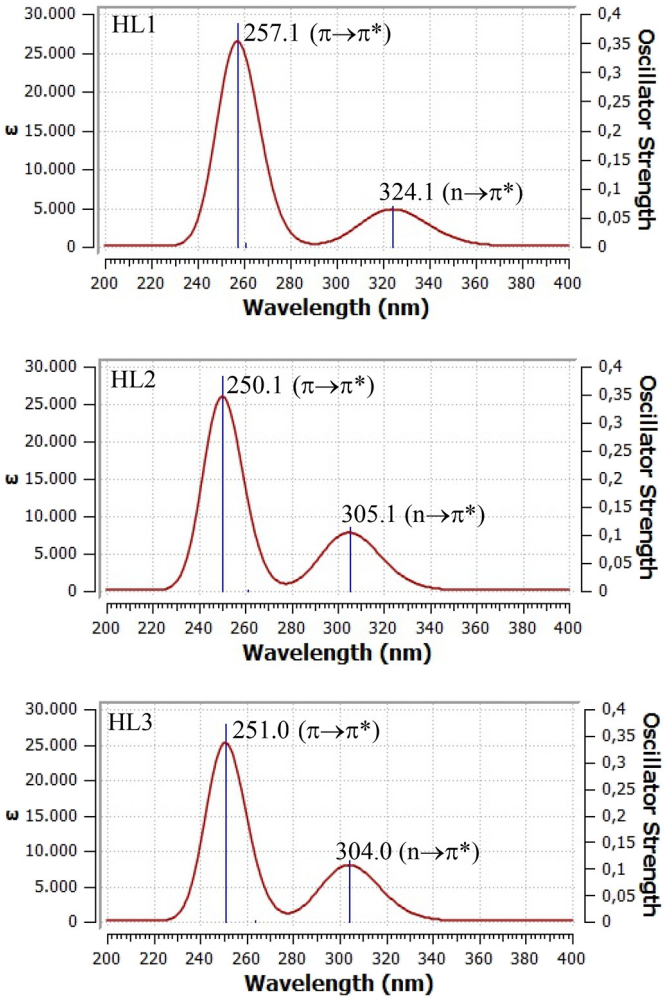

Fig. 4. Calculated UV–Vis spectra of HL1, HL2 and HL3 Schiff bases calculated at TD-DFT/B3LYP/6-31G(d) level in aqueous phase.

the substituents have an inductive effect close to each other. Because stronger electron withdrawing groups reduce the shielding on the neighboring nucleus and cause it to peak at high ppm. According to these data obtained in the aqueous phase, CH_3O can be considered as electron withdrawing group (EWG), whereas CH_3 and Cl can be taken into account as electron donating groups (EDG).

3.5. UV-VIS spectrums and labeling of bands

UV-VIS spectra and electronic transitions can be estimated by time-dependent density functional theory (TD-DFT) calculations [48]. Since the molecules containing certain functional groups form bands at characteristic wavelengths, electronic spectroscopy can also provide support in molecular structure prediction. In this study, electronic spectra of HL1, HL2 and HL3 Schiff bases were calculated at TD-DFT/B3LYP/6-31G(d) level in the aqueous phase and UV–Vis spectrums of Schiff bases are given in Fig. 4. TD-DFT calculations were made according to default settings of Gaussian 09. Default setting of the program contains Nstate = 6, root = 1. Nstate = 6 indicates that six states are taken into account in TD-DFT calculations, three of which are singlets and three are triplets. Root = 1 is the first excited state.

As seen in Fig. 4, two bands are observed in the electronic spectrum of each of the Schiff bases. The shapes of the bands in the electronic spectrum are quite similar. Only the HL1 spectrum differs slightly from the HL2 and HL3 spectrum in terms of the wavelengths of the bands. The wavelengths of the bands of the HL2 and HL3 molecules are also quite close to each other. This result is also compatible with ^{13}C NMR spectrum data. The similarity of the bands shapes and the close wavelengths show that the structures of the studied molecules are quite similar.

To determine the transitions forming the bands in the electronic spectrum, transition coefficients for each excitation were examined in the account output files. It was determined that mainly low wavelength bands consist of HOMO-1 → LUMO and high wavelength bands consist of HOMO → LUMO transitions. Orbital character of HOMO-1, HOMO and LUMO can be estimated from theirs contour diagrams. Therefore, contour diagrams of the frontier orbitals of HL1, HL2 and HL3 were obtained and given in Fig. 5.

As can be seen from Fig. 5, HOMO-1 shows π-molecular orbitals on the azomethine group and benzene ring. LUMO indicates π*-molecular orbitals on the benzene ring and π-molecular orbitals of azomethine group. HOMO shows π-molecular orbitals on the benzene ring and orbitals that do not bond on the nitrogen atom. According to this finding, it can be said that the HOMO-1 → LUMO transition is a π → π* transition and the HOMO → LUMO transition is an n → π* transition. This electronic transition labeling is given in Fig. 4.

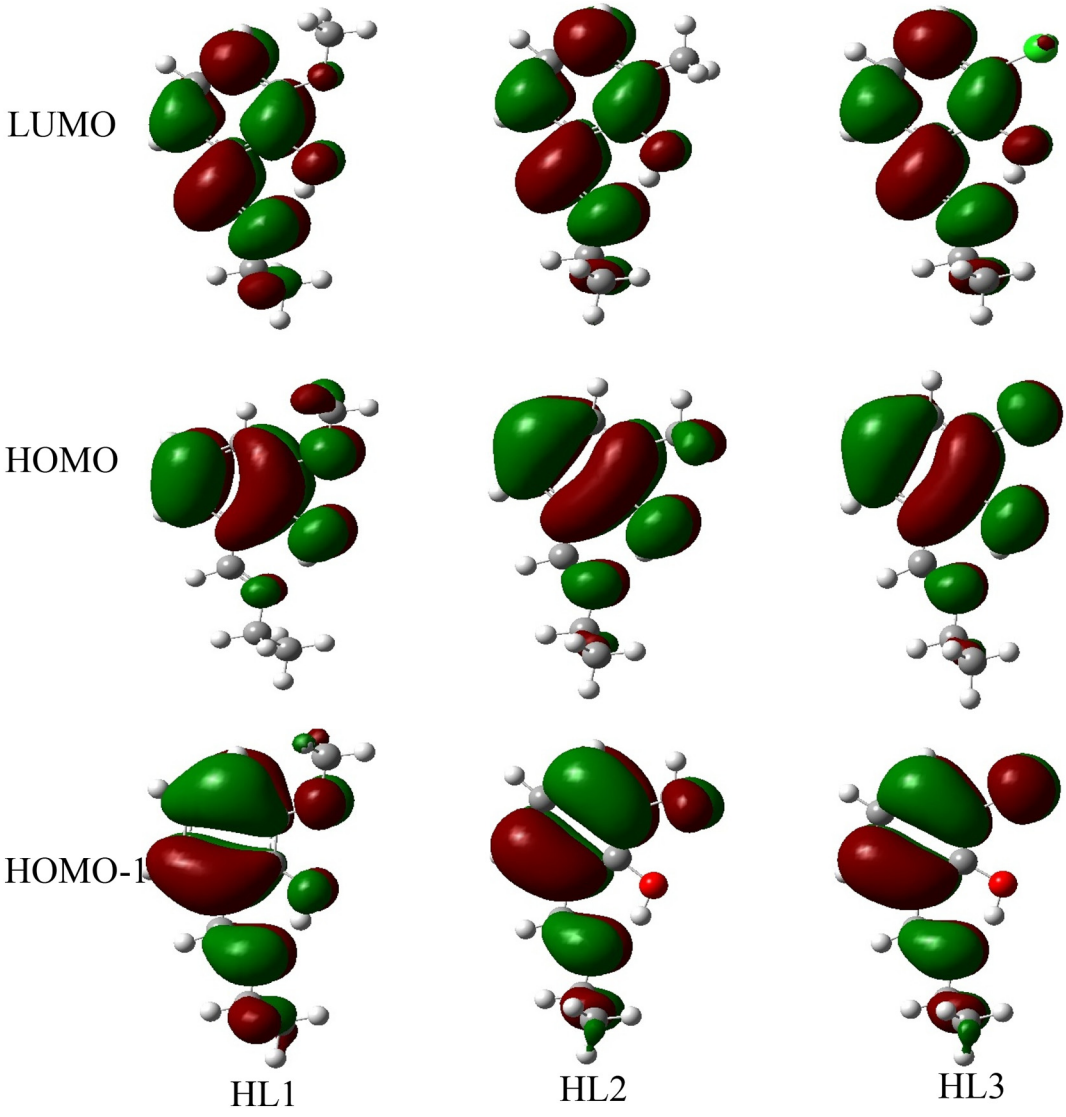

Fig. 5. Contour diagrams of frontier orbitals for HL1, HL2 and HL3 Schiff bases.

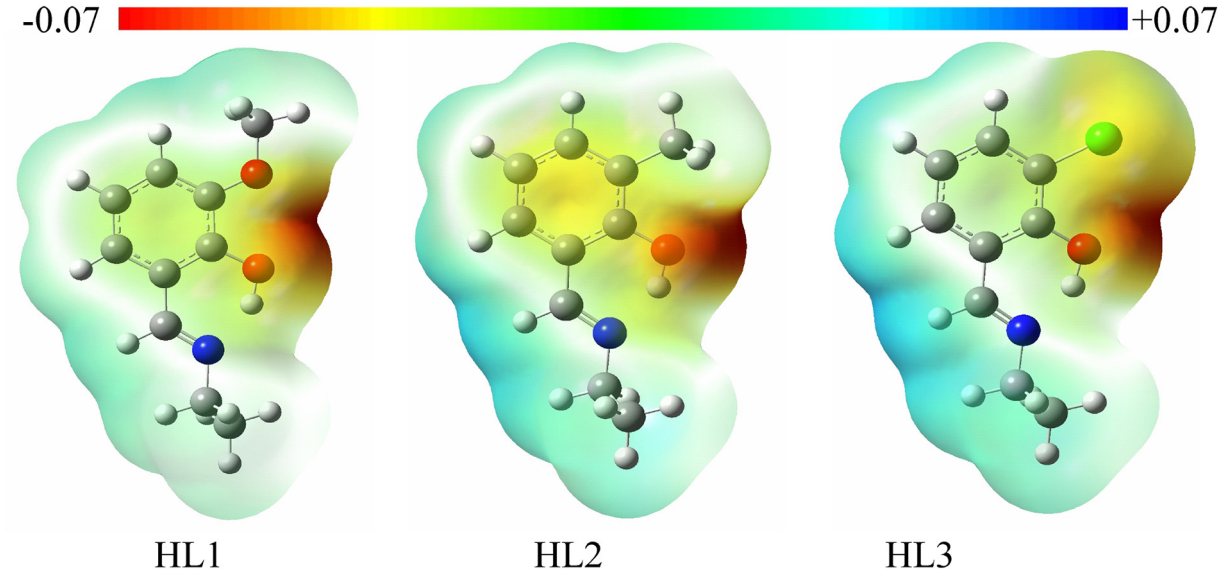

Fig. 6. MEP maps of Schiff bases obtained at B3LYP/6-31G(d) level in aqueous phase.

3.6. Molecular electrostatic potential (MEP) maps

The electronic properties of molecules can be estimated by calculating molecular orbital energy diagrams (MOED), contour diagrams of molecular orbitals, molecular electrostatic potential (MEP) maps and electronic charges of atoms [49]. Because Schiff bases form complexes with transition metals, donor atoms can be estimated from MEP maps. Regions with high and low electron density can be easily seen from MEP maps. MEP maps of the studied Schiff bases were calculated in the aqueous phase and given in Fig. 6.

As seen in Fig. 6, the region with the highest electron density is around O17 and N11. This region is sensitive to nucleophilic attacks. Schiff bases are expected to bind to transition metals from this region. According to ^{13}C NMR chemical shift data, it was stated that CH_3O is EWG, CH_3 and Cl are EDG. It is seen that the CH_3O, OH and N region in HL1 is darker red than the CH_3, OH and N region in HL2 and the Cl, OH and N region in HL3. Therefore, HL1 Schiff base is more susceptible to nucleophilic attacks than HL2 and HL3.

3.7. Some molecular properties of Schiff bases

The easiest way to estimate molecular properties in computational chemistry is to calculate molecular descriptors. A large number of molecular descriptors can be calculated. By comparing the calculated properties of similar molecules, the substitution effect can be interpreted [49]. In order to predict the substituents effect, molecular structural descriptors of Schiff base such as ionization energy (I), electron affinity (A), energy gap (ΔE), hardness (η), electronegativity (χ) and electrophilicity index (ω) were calculated from Eqs. (1)–(6). Static dipole moment (μ) and average linear polarizability (α) were taken from the calculation output files. To estimate the antitumor-antibacterial activity of studied Schiff bases, the same molecular structure identifiers were calculated for 5-FU used as an anticancer drug and SHA used as an antibacterial drug and their numerical values are given in Table 5.

As seen in Table 5, I, A, ΔE, η, χ and ω values of Schiff bases increase in HL1 < HL2 < HL3 order. ^{13}C NMR chemical shift values indicated that CH_3O is an electron withdrawing group (EWG). Thus, it can be said that the I, A, ΔE, η, χ and ω values of Schiff bases containing electron attracting groups such as CH_3O are low. On the other hand, the static dipole moment of HL3 is considerably larger than HL1 and HL2, and its average molecular polarizability is very close to that of HL2. The average molecular polarizability depends on the molecular size and hardness. The average molecular polarizability of HL2 and HL3 being close indicates that the sizes of CH_3 and Cl are close.

In addition, the molecular structure descriptors of 5-FU and SHA are close to molecular structure descriptors of Schiff bases in size. Molecular structure descriptors of Schiff bases and 5FU were compared to predict antitumor activity. Molecular structure descriptors of Schiff bases and SHA were compared to determine their antibacterial activity. Comparison of the molecular descriptors of Schiff bases with 5-FU and SHA are given in Table 6.

As seen in Table 6, some descriptors of Schiff bases are smaller than those of 5-FU and some are larger. In fact, the values of the ω and μ descriptors of the 5-FU are among the values of the Schiff bases. These findings indicate that if 5-FU is used as antitumor drug, the Schiff

Table 5
Some molecular descriptors calculated at the B3LYP/6-31G(d) level for the HL1, HL2, HL3, 5FU and SHA in the aqueous phase.

Descriptors	HL1	HL2	HL3	5-FU	SHA
E_{HOMO}[a]	−5.654	−5.910	−6.203	−6.612	−5.665
E_{LUMO}[a]	−1.256	−1.250	−1.511	−1.224	−1.535
I[a]	5.654	5.910	6.203	6.612	5.665
A[a]	1.256	1.250	1.511	1.224	1.535
ΔE[a]	4.398	4.660	4.693	5.388	4.130
η[a]	2.199	2.330	2.346	2.694	2.065
χ[a]	3.455	3.580	3.857	3.918	3.600
ω[a]	2.714	2.750	3.170	2.849	3.138
μ[b]	2.921	2.906	5.937	5.238	1.605
α[c]	164.7	159.2	158.9	71.8	219.1

[a] eV.
[b] Debye.
[c] a.u.

Table 6
Comparison of the relationship between the molecular descriptors of HL1, HL2, HL3 Schiff bases and the molecular descriptors of 5-FU and SHA.

Descriptors	Antitumor activity	Descriptors	Antibacterial activity
I, ΔE, η, χ	HL1 < HL2 < HL3 < 5-FU	I	HL1 < SHA < HL2 < HL3
A	5-FU < HL2 < HL1 < HL3	A	HL2 < HL1 < HL3 < SHA
ω	HL1 < HL2 < 5-FU < HL3	ΔE, η	SHA < HL1 < HL2 < HL3
μ	HL2 < HL1 < 5-FU < HL3	χ, ω	HL1 < HL2 < SHA < HL3
α	5-FU < HL3 < HL2 < HL1	μ	SHA < HL2 < HL1 < HL3
		α	HL3 < HL2 < HL1 < SHA

bases examined may also have antitumor activity. A similar interpretation can be made for the antibacterial activity.

3.8. Molecular docking: antitumor and antibacterial activity prediction

Molecular docking process allows to examine the biological activity of molecules at the molecular level and is one of the popular techniques used in the identification and development of drug candidate molecules. The interactions between the structure of the cell lines minimized at the molecular level with the molecular docking process and the drug candidate compound can be examined at the molecular level. By doing molecular docking, binding energies, binding modes, and types of secondary chemical interactions between the target protein and the molecule examined can be determined.

In this study, Schiff bases investigated were docked against the MCF-7 breast cancer cell line and the H37Rv tuberculosis bacterial cell line. Anticancer and antibacterial properties of Schiff bases were investigated. PDB ID for the target protein representing the MCF-7 breast cancer cell line was determined as 1JNX. 1JNX is the protein that is associated with breast cancer and represents the BRCA1 region of the BRCT crystal structure. BRCA1 is the region containing approximately 90–100 amino acid sequence repeats of the C-terminal region. The C-terminal region in BRCA1 occurs with mutations that cause early-onset breast cancer. This area is very important for tumor suppression. Amino acid repeats in BRCT are very important in DNA repair [50].

The highly contagious tuberculosis disease is caused by the infection of *Mycobacterium tuberculosis* (Mtb) agent. Proteins created by targeting the basic enzymes of Mtb are quite high. Most importantly, the aspartate semialdehyde dehydrogenase (ASADH) enzyme, encoded by the aspartate β-semialdehyde (ASA) gene. 3TZ6 is the crystal structure of *Mycobacterium tuberculosis* H37Rv inhibitor and aspartate semialdehyde dehydrogenase complexed with phosphate [51].

In this study, HL1, HL2 and HL3 Schiff bases were docked against the MCF-7 (PDB ID: 1JNX) breast cancer cell line and against the H37Rv (PDB ID: 3TZ6) tuberculosis bacteria cell line and docking poses are given in Fig. 7.

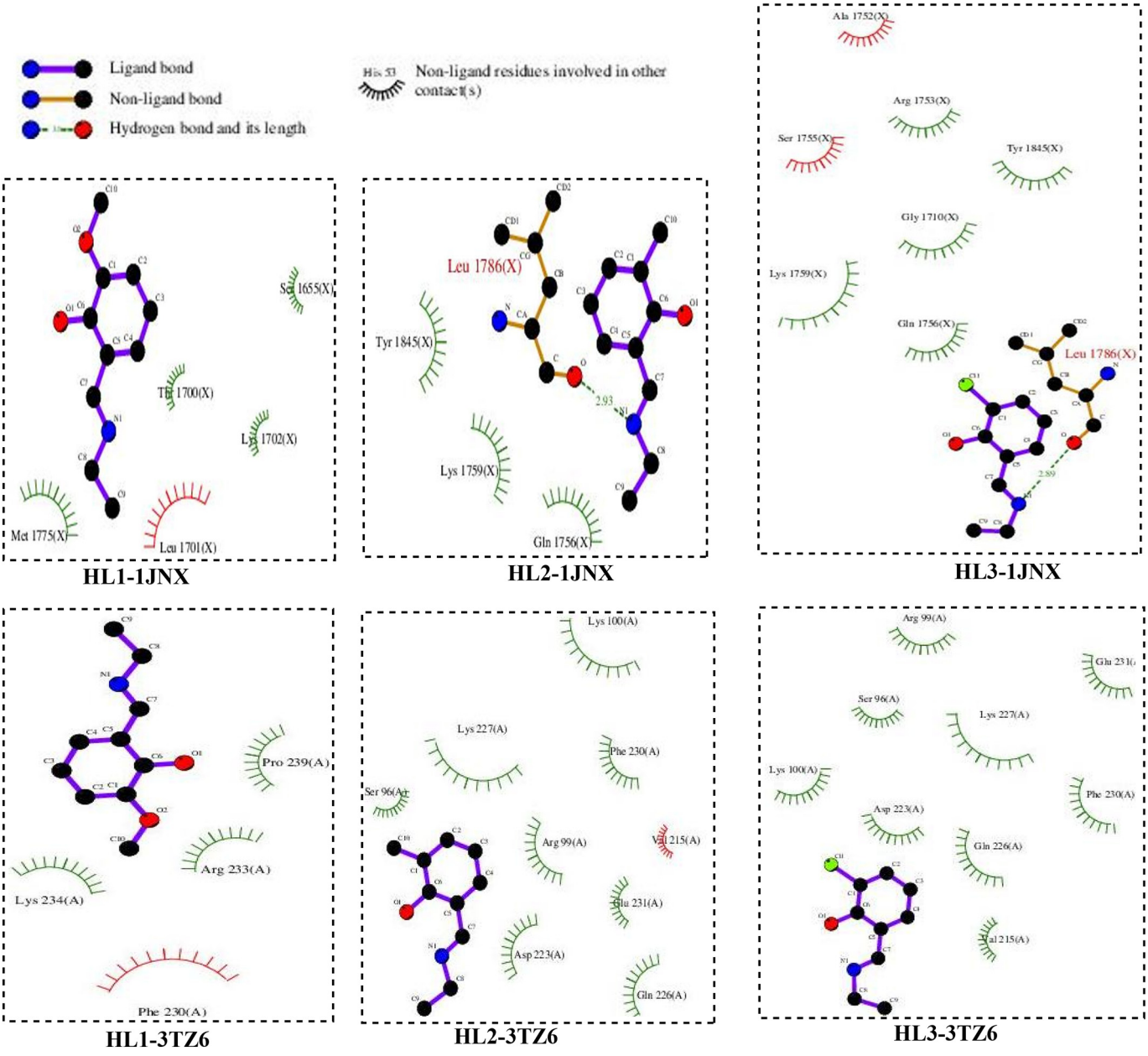

Fig. 7. Docking poses of investigated Schiff bases and target proteins.

Table 7
Interaction types between HL1-HL3 and 1JNX and 3TZ6 target proteins.

	Hydrophobic	Polar	pi-pi	H-bonds	Halogen-bond
HL1-1JNX	MET1775 LEU1701	–	–	–	–
HL2-1JNX	LEU1786	LYS1759	TYR1845	LEU1786	–
HL3-1JNX	LEU1786	LYS1759	TYR1845	LEU1786	GLY1710 ALA1752 ARG1753 SER1755
5-FU-1JNX	–	LYS1702	–	SER1655	–
HL1-3TZ6	PRO239	ARG233	PHE230	–	–
HL2-3TZ6	VAL215	LYS100 GLN226	PHE230	–	–
HL3-3TZ6	VAL215	–	PHE230	–	GLU231
SHA-3TZ6	PHE230	ARG233	PHE230	–	–

The interaction types between Schiff bases and target proteins given docking poses in Fig. 7 are presented in Table 7.

As seen in Table 7, HL3 Schiff base is the most interacting with the 1JNX target protein. HL3 molecule formed hydrophobic with amino acid residue LEU1786, polar with LYS1759, pi-pi interaction with TYR1845, H-bond with LEU1786, and halogen bond with amino acid residues GLY1710, ALA1752, ARG1753 and SER1755. Schiff base, which interacts more strongly with the 3TZ6 protein, is difficult to determine from Table 7. Because the Schiff bases examined interact with the same number of amino acid residues.

Binding energy (BE), intermolecular energy (IE), van der Waals, H-bond, desolve energy (WHDE), interaction surface (IS) and inhibition constant (Ki) were calculated for prediction anticancer and antibacterial activities of Schiff bases. Their values along with the values of the references are given in Table 8.

As seen in Table 8, BE, IE and WHDE values between Schiff bases and 1JNX, 3TZ6 proteins are lower than reference materials. These energies are components of interaction energies between the ligand and the target protein. More negative interaction energy indicates higher inhibition efficiency. Given the energies, the inhibition efficiency of Schiff bases is higher than the references. According to these energies, the molecules studied can be drug candidate molecules for both breast cancer cell line and *Mycobacterium tuberculosis* cell line.

On the other hand, the interaction surfaces (IS) of Schiff bases appear to be higher than the interaction surfaces of the references. The high interaction surface also increases the ligand-protein interaction and leads to increased anticancer, antibacterial activity. According to IS values anticancer and antibacterial activities of Schiff bases are higher than the references.

Inhibition constant (Ki) is a data on the amount of drug to be used in treatment. The smaller Ki value, the less the amount of drug used in treatment [52]. The Ki values of HL2 and HL3 Schiff bases are smaller than the reference and the Ki value of HL1 is greater than the reference. This result shows that the inhibition efficiency of HL3 Schiff base is highest.

Table 8
Calculated docking results between HL1-HL3 and 1JNX and 3TZ6 target proteins.

	BE[a]	IE[a]	WHDE[a]	IS	Ki[b]
HL1-1JNX	−3.74	−4.35	−4.31	439.89	1800.0
HL2-1JNX	−4.59	−5.49	−5.29	440.74	431.15
HL3-1JNX	−4.69	−5.56	−5.34	444.86	382.48
5-FU-JNX	−3.69	−3.69	−3.63	247.98	664.86
HL1-3TZ6	−3.74	−4.24	−4.23	407.22	1820.0
HL2-3TZ6	−4.38	−5.26	−5.13	471.68	612.00
HL3-3TZ6	−4.40	−4.86	−4.82	469.43	598.76
SHA-3TZ6	−3.61	−3.93	−3.97	272.60	716.81

[a] Kcal/mol.
[b] μM in unit.

As a result, it was found that the examined Schiff bases showed anticancer and antibacterial properties and had a higher activity than references. Moreover, it can be seen from Table 8 that hypothetical HL2 and HL3 Schiff bases have higher activity than experimentally synthesized HL1. The activity rank of Schiff bases against 1JNX cancer cell line was found as HL1 < HL2 < HL3. This sequence is the same as that of the molecular identifiers I, A, ΔE, η, χ and ω. It seems difficult to give an activity ranking against the 3TZ6 bacterial cell line. However, it can be said that HL2 and HL3 are more active than HL1.

4. Results

Molecular structures, spectroscopic properties, molecular electrostatic potential maps and some molecular properties of HL1, HL2 and HL3 Schiff bases were investigated in the aqueous phase at B3LYP/6-31G(d) level. It was determined that CH_3O has higher electron withdrawing group than CH_3 and Cl substituents. Schiff bases were docked against the MCF7 breast cancer cell line. All of Schiff bases examined were found to have higher activity than the reference 5-FU. In addition, Schiff bases examined were docked against the H37Rv tuberculosis bacteria cell line. Docking results were compared with the antibacterial standard SHA and Schiff bases were found to have higher antibacterial activity than SHA. Antibacterial activity of HL2 and HL3 molecules was found to be higher than HL1. It was predicted that the binding of electron donating group to the ortho position of the hydroxyl group in studied Schiff bases increased both antitumor and antibacterial activity.

CRediT authorship contribution statement

The authors have made the following contributions to this article.

Serpil Kaya: The calculation of optimized molecular structures, spectroscopic properties (IR, ^{1}H NMR and ^{13}C NMR, UV-VIS), molecular electrostatic potential maps and some molecular properties of HL1, HL2HL3 Schiff bases.

Sultan Erkan: Docking of HL1, HL2 and HL3 Schiff bases against MCF7 cancer cell line and H37Rv mycobacterium tuberculosis cell line.

Duran Karakaş: Design of HL1, HL2 and HL3 Schiff base molecules, the collection and interpretation of all calculation results and writing of the article.

Declaration of competing interest

The authors declare that they have no known competing financial interests or personal relationships that could have appeared to influence the work reported in this paper.

Acknowledgments

The authors are grateful for their support to the Sivas Cumhuriyet University, Scientific Research Unit (Project No: F-629).

References

[1] H. Schiff, Mittheilungen aus dem Universitätslaboratorium in Pisa: eine neue Reihe organischer Basen, Justus Liebigs Annalen der Chemie 131 (1) (1864) 118–119.

[2] Z. Shokohi-Pour, H. Chiniforoshan, M.R. Sabzalian, S.A. Esmaeili, A.A. Momtazi-borojeni, Cobalt (II) complex with novel unsymmetrical tetradentate Schiff base (ON) ligand: in vitro cytotoxicity studies of complex, interaction with DNA/protein, molecular docking studies, and antibacterial activity, J. Biomol. Struct. Dyn. 36 (2) (2018) 532–549.

[3] Z.H. Chohan, S.H. Sumrra, M.H. Youssoufi, T.B. Hadda, Metal based biologically active compounds: design, synthesis, and antibacterial/antifungal/cytotoxic properties of triazole-derived Schiff bases and their oxovanadium (IV) complexes, Eur. J. Med. Chem. 45 (7) (2010) 2739–2747.

[4] P. Ghorai, R. Saha, S. Bhuiya, S. Das, P. Brandão, D. Ghosh, ... A. Saha, Syntheses of Zn (II) and Cu (II) Schiff base complexes using N, O donor Schiff base ligand: crystal structure, DNA binding, DNA cleavage, docking and DFT study, Polyhedron 141 (2018) 153–163.

[5] Z. Kazemi, H.A. Rudbari, M. Sahihi, V. Mirkhani, M. Moghadam, S. Tangestaninejad, ... S. Gharaghani, Synthesis, characterization and biological application of four novel metal-Schiff base complexes derived from allylamine and their interactions with human serum albumin: Experimental, molecular docking and ONIOM computational study, Journal of Photochemistry and Photobiology B: Biology 162 (2016) 448–462.

[6] D.N. Dhar, C.L. Taploo, Schiff-bases and their applications, J. Sci. Ind. Res. 41 (8) (1982) 501–506.

[7] P. Przybylski, A. Huczynski, K. Pyta, B. Brzezinski, F. Bartl, Biological properties of Schiff bases and azo derivatives of phenols, Curr. Org. Chem. 13 (2) (2009) 124–148.

[8] G. Bringmann, M. Dreyer, J.H. Faber, P.W. Dalsgaard, D. Stærk, J.W. Jaroszewski, ... S.B. Christensen, Ancistrotanzanine C and Related 5, 1′-and 7, 3′-Coupled naphthylisoquinoline Alkaloids from Ancistrocladus tanzaniensis, Journal of natural products 67 (5) (2004) 743–748.

[9] A.O.D. Souza, F. Galetti, C.L. Silva, B. Bicalho, M.M. Parma, S.F. Fonseca, ... M. Andrade-Neto, Antimycobacterial and cytotoxicity activity of synthetic and natural compounds, Quím. Nova 30 (7) (2007) 1563–1566.

[10] Z. Guo, R. Xing, S. Liu, Z. Zhong, X. Ji, L. Wang, P. Li, Antifungal properties of Schiff bases of chitosan, N-substituted chitosan and quaternized chitosan, Carbohydr. Res. 342 (10) (2007) 1329–1332.

[11] Gary L. Miessler, Donald Arthur Tarr, Inorg. Chem. (1999) 338.

[12] L. Kang, L. Zhao, S. Yao, C. Duan, A new architecture of super-hydrophilic β-SiAlON/graphene oxide ceramic membrane for enhanced anti-fouling and separation of water/oil emulsion, Ceram. Int. 45 (2019) 16717.

[13] X. Feng, Y.Q. Feng, J.J. Chen, S.W. Ng, L.Y. Wang, J.Z. Guo, Reticular three-dimensional 3d–4f frameworks constructed through substituted imidazole-dicarboxylate: syntheses, luminescence and magnetic properties study, Dalton Trans. 44 (2) (2015) 804–816.

[14] C. Duan, F. Li, M. Yang, H. Zhang, Y. Wu, H. Xi, Rapid synthesis of hierarchically structured multifunctional metal–organic zeolites with enhanced volatile organic compounds adsorption capacity, Ind. Eng. Chem. Res. 57 (45) (2018) 15385–15394.

[15] X. Feng, L.F. Ma, L. Liu, L.Y. Wang, H.L. Song, S.Y. Xie, A series of heterometallic three-dimensional frameworks constructed from imidazole–dicarboxylate: structures, luminescence, and magnetic properties, Cryst. Growth Des. 13 (10) (2013) 4469–4479.

[16] Y. Yang, L. Kang, H. Li, Enhancement of photocatalytic hydrogen production of BiFeO3 by Gd3+ doping, Ceram. Int. 45 (6) (2019) 8017–8022.

[17] X. Feng, L.Y. Wang, J.S. Zhao, J.G. Wang, N.S. Weng, B. Liu, X.G. Shi, Series of anion-directed lanthanide-rigid-flexible frameworks: syntheses, structures, luminescence and magnetic properties, CrystEngComm 12 (3) (2010) 774–783.

[18] M McQuade, R., Stojanovska, V., C C Bornstein, J., & Nurgali, K. (2017). Colorectal cancer chemotherapy: the evolution of treatment and new approaches. Curr. Med. Chem., 24(15), 1537–1557.

[19] M. Zhang, C. Saint-Germain, G. He, R.W.Y. Sun, Drug delivery systems for anti-cancer active complexes of some coinage metals, Curr. Med. Chem. 25 (4) (2018) 493–505.

[20] W.F. De Azevedo, Y.P. Mascarenhas, G.F. De Sousa, C.A.L. Filgueiras, cis-[1, 2-Bis (propylsulfinyl) ethane-S, S′] dichloroplatinum (II), Acta Crystallogr. Sect. C: Cryst. Struct. Commun. 51 (4) (1995) 619–621.

[21] A.M. Florea, D. Büsselberg, Cisplatin as an anti-tumor drug: cellular mechanisms of activity, drug resistance and induced side effects, Cancers 3 (1) (2011) 1351–1371.

[22] P.C. Bruijnincx, P.J. Sadler, New trends for metal complexes with anticancer activity, Curr. Opin. Chem. Biol. 12 (2) (2008) 197–206.

[23] I.B. Amali, M.P. Kesavan, V. Vijayakumar, N.I. Gandhi, J. Rajesh, G. Rajagopal, Structural analysis, antimicrobial and cytotoxic studies on new metal (II) complexes containing N2O2 donor Schiff base ligand, J. Mol. Struct. 1183 (2019) 342–350.

[24] C. Kachi-Terajima, T. Shimoyama, T. Ishigami, M. Ikeda, Y. Habata, A hemiaminal–ether structure stabilized by lanthanide complexes with an imidazole-based Schiff base ligand, Dalton Trans. 47 (8) (2018) 2638–2645.

[25] J. Zhang, L. Xu, W.Y. Wong, Energy materials based on metal Schiff base complexes, Coord. Chem. Rev. 355 (2018) 180–198.

[26] K. Sayin, A. Üngördü, Investigation of anticancer properties of caffeinated complexes via computational chemistry methods, Spectrochim. Acta A Mol. Biomol. Spectrosc. 193 (2018) 147–155.

[27] V. Torabi, H. Kargar, A. Akbari, R. Behjatmanesh-Ardakani, H. Amiri Rudbari, M. Nawaz Tahir, Nickel (II) complex with an asymmetric tetradentate Schiff base ligand: synthesis, characterization, crystal structure, and DFT studies, J. Coord. Chem. 71 (22) (2018) 3748–3762.

[28] S. Erkan, D. Karakaş, Computational investigation of structural, nonlinear optical and anti-tumor properties of dinuclear metal carbonyls bridged by pyridyl ligands with alkyne unit, J. Mol. Struct. 1199 (2020) 127054.

[29] N. Gövdeli, D. Karakaş, Quantum chemical studies on hypothetical Fischer type Mo (CO)5[C(OEt)Me] and Mo(CO)5[C(OMe)Et] carbene complexes, J. Mol. Struct. 1163 (2018) 94–102.

[30] D. Wu, L. Guo, S.J. Li, Synthesis, structural characterization and anti-breast cancer activity evaluation of three new Schiff base metal (II) complexes and their nanoparticles, J. Mol. Struct. 1199 (2020) 126938.

[31] R.D. Dennington, T.A. Keith, J.M. Millam, GaussView 6.0. 16, Semichem. Inc., Shawnee Mission KS, 2016.

[32] M.J. Frisch, G.W. Trucks, H.B. Schlegel, G.E. Scuseria, M.A. Robb, J.R. Cheeseman, ... H. Nakatsuji, Gaussian09 Revision D. 01, Gaussian Inc., Wallingford CT, 2009 , See also: URL: http://www.gaussian.com.

[33] Ş. Güveli, N. Özdemir, T. Bal-Demirci, B. Ülküseven, M. Dinçer, Ö. Andaç, Quantum-chemical, spectroscopic and X-ray diffraction studies on nickel complex of 2-hydroxyacetophenone thiosemicarbazone with triphenylphosphine, Polyhedron 29 (12) (2010) 2393–2403.

[34] A.D. Becke, Density-functional exchange-energy approximation with correct asymptotic behavior, Phys. Rev. A 38 (6) (1988) 3098.

[35] V.A. Rassolov, M.A. Ratner, J.A. Pople, P.C. Redfern, L.A. Curtiss, 6-31G* basis set for third-row atoms, J. Comput. Chem. 22 (9) (2001) 976–984.

[36] M. Cossi, V. Barone, Analytical second derivatives of the free energy in solution by polarizable continuum models, J. Chem. Phys. 109 (15) (1998) 6246–6254.

[37] J.A. Bohmann, F. Weinhold, T.C. Farrar, Natural chemical shielding analysis of nuclear magnetic resonance shielding tensors from gauge-including atomic orbital calculations, J. Chem. Phys. 107 (4) (1997) 1173–1184.

[38] D. Guillaumont, S. Nakamura, Calculation of the absorption wavelength of dyes using time-dependent density-functional theory (TD-DFT), Dyes Pigments 46 (2) (2000) 85–92.

[39] P. Rawat, R.N. Singh, Experimental and theoretical study of 4-formyl pyrrole derived aroylhydrazones, J. Mol. Struct. 1084 (2015) 326–339.

[40] R.G. Pearson, Absolute electronegativity and hardness: application to inorganic chemistry, Inorg. Chem. 27 (4) (1988) 734–740.

[41] C.M. Da Silva, D.L. da Silva, L.V. Modolo, R.B. Alves, M.A. de Resende, C.V. Martins, Â. de Fátima, Schiff bases: a short review of their antimicrobial activities, J. Adv. Res. 2 (1) (2011) 1–8.

[42] Z. Bikadi, E. Hazai, Application of the PM6 semi-empirical method to modeling proteins enhances docking accuracy of AutoDock, J. Cheminform. 1 (1) (2009) 15.

[43] I.M. Alecu, J. Zheng, Y. Zhao, D.G. Truhlar, Computational thermochemistry: scale factor databases and scale factors for vibrational frequencies obtained from electronic model chemistries, J. Chem. Theory Comput. 6 (9) (2010) 2872–2887.

[44] J. Kovacic, The C=N stretching frequency in the infrared spectra of Schiff's base complexes-I. Copper complexes of salicylidene anilines, Spectrochim. Acta A: Mol. Spectrosc. 23 (1) (1967) 183–187.

[45] J.R. Bowser, Inorganic Chemistry, Brooks, 1993 721–725.

[46] D. Sinha, A.K. Tiwari, S. Singh, G. Shukla, P. Mishra, H. Chandra, A.K. Mishra, Synthesis, characterization and biological activity of Schiff base analogues of indole-3-carboxaldehyde, Eur. J. Med. Chem. 43 (1) (2008) 160–165.

[47] Y.S. Kara, S. Yalduz, Substituent effect study on the experimental 13C NMR chemical shifts of 3-(substituted phenyl)-3a, 4, 8, 8a-tetrahydro-1, 3-dioxepino [5, 6-d][1,2] isoxazoles, J. Mol. Struct. 1193 (2019) 158–165.

[48] P.F. Santiago, J.R.S. Mercado, B.M. Brito, DFT/TD-DFT studies on electronic and photophysical properties of Auranofin: a reference Au(I) complex, Polyhedron 180 (2020) 114262.

[49] K. Sayin, Research of the substituent effect on non-linear optical properties of bis (difluoroboron)-1, 2-bis ((1H-pyrrol-2-yl) methylene) hydrazine (BOPHY) derivatives: molecular simulation analyses, Spectrochim. Acta A Mol. Biomol. Spectrosc. 212 (2019) 380–387.

[50] R.S. Williams, R. Green, J.M. Glover, Crystal structure of the BRCT repeat region from the breast cancer-associated protein BRCA1, Nat. Struct. Biol. 8 (10) (2001) 838–842.

[51] R. Vyas, R. Tewari, M.S. Weiss, S. Karthikeyan, Structures of ternary complexes of aspartate-semialdehyde dehydrogenase (Rv3708c) from Mycobacterium tuberculosis H37Rv, Acta Crystallogr. D Biol. Crystallogr. 68 (6) (2012) 671–679.

[52] R. Merugu, U.K. Neerudu, K. Dasa, K.V. Singh, Molecular docking studies of deacetylbisacodyl with intestinal sucrase-maltase enzyme, Int. J. Adv. Sci. Res. 2 (12) (2016) 191–193.